Published as: *J Neurophysiol*. 2004 January ; 91(1): 194–205.

Influence of Ionic Conductances on Spike Timing Reliability of Cortical Neurons for Suprathreshold Rhythmic Inputs

Susanne Schreiber[1,5], **Jean-Marc Fellous**[2], **Paul Tiesinga**[1,3], and **Terrence J. Sejnowski**[1,2,4]

[1] Sloan-Swartz Center for Theoretical Neurobiology, Salk Institute, La Jolla, California 92037

[2] Howard Hughes Medical Institute, and Computational Neurobiology Lab, Salk Institute, La Jolla, California 92037

[3] Department of Physics and Astronomy, University of North Carolina, Chapel Hill, North Carolina 27599

[4] Department of Biology, University of California San Diego, La Jolla, California 92037

[5] Institute for Theoretical Biology, Humboldt-University Berlin, D-10115 Berlin, Germany

Abstract

Spike timing reliability of neuronal responses depends on the frequency content of the input. We investigate how intrinsic properties of cortical neurons affect spike timing reliability in response to rhythmic inputs of suprathreshold mean. Analyzing reliability of conductance-based cortical model neurons on the basis of a correlation measure, we show two aspects of how ionic conductances influence spike timing reliability. First, they set the preferred frequency for spike timing reliability, which in accordance with the resonance effect of spike timing reliability is well approximated by the firing rate of a neuron in response to the DC component in the input. We demonstrate that a slow potassium current can modulate the spike timing frequency preference over a broad range of frequencies. This result is confirmed experimentally by dynamic-clamp recordings from rat prefrontal cortical neurons in vitro. Second, we provide evidence that ionic conductances also influence spike timing beyond changes in preferred frequency. Cells with the same DC firing rate exhibit more reliable spike timing at the preferred frequency and its harmonics if the slow potassium current is larger and its kinetics are faster, whereas a larger persistent sodium current impairs reliability. We predict that potassium channels are an efficient target for neuromodulators that can tune spike timing reliability to a given rhythmic input.

INTRODUCTION

Intrinsic neuronal properties, such as their biochemistry, the distribution of ion channels, and cell morphology contribute to the electrical responses of cells (see e.g. Goldman et al. 2001; Magee 2002; Mainen and Sejnowski 1996; Marder et al. 1996; Turrigiano et al. 1994). In this study we explore the influence of ionic conductances on the reliability of the timing of spikes of cortical cells. Robustness of spike timing to physiological noise is the prerequisite for a spike timing–based code, and has recently been investigated (Beierholm et al. 2001; Brette and Guigon 2003; Fellous et al. 2001; Fricker and Miles 2000; Gutkin et al. 2003; Mainen and Sejnowski 1995; Reinagel and Reid 2002; Tiesinga et al. 2002). It has been found experimentally that different types of neurons are tuned to different stimuli with respect to spike timing reliability. For example, cortical interneurons show maximum reliability in

Address for reprint requests and other correspondence: T. J. Sejnowski, Computational Neurobiology Laboratory, The Salk Institute, 10010 N. Torrey Pines Road, La Jolla, CA 92037 (terry@salk.edu).

response to higher-frequency sinusoidal stimuli, whereas pyramidal cells respond more reliably to lower-frequency sinusoidal inputs (Fellous et al. 2001). An important difference between those types of neurons is the composition of their ion channels. Taking into account that effective numbers of ion channels can be adjusted on short time scales through neuromodulation, changes in ion channels may also provide a useful way for a neuron to dynamically maximize spike timing reliability according to the properties of the input.

Spike timing reliability is enhanced with increasing stimulus amplitude (Mainen and Sejnowski 1995). In the intermediate amplitude regime, the frequency content of the stimulus is an important factor determining reliability (Fellous et al. 2001; Haas and White 2002; Hunter and Milton 2003; Hunter et al. 1998; Jensen 1998; Nowak et al. 1997; Tiesinga 2002). Spike timing reliability of a neuron is maximal for those stimuli that contain frequencies matching the intrinsic frequency of a neuron (Hunter et al. 1998). The intrinsic (or preferred) frequency is given by the firing rate of a neuron in response to the DC component of the stimulus. Because of the relation to the DC firing rate of a neuron, both the DC value (whether the stimulus mean or additional synaptic input) and the conductances of a cell can be expected to influence the spike timing frequency preference. The former was recently shown by Hunter and Milton (2003). The influence of conductances (rather than injected current) on spike timing reliability through changes in the neuronal activity according to the resonance effect is the focus of the first part of this paper, see RESULTS (*Influence of conductances on the frequency preference*).

In this part we specifically seek to understand which ionic conductances of cortical neurons can mediate changes of the preferred frequency (with respect to spike timing reliability) over a broad range of frequencies. Reliability is assessed on the basis of the robustness of spike timing to noise (of amplitude smaller than the stimulus amplitude). Injecting sinusoidal currents on top of a DC current into conductance-based model neurons, we confirm that spike timing reliability is frequency-dependent as predicted by the resonance effect. We show that reliability can be regulated at the level of ion channel populations, and identify the slow potassium channels as powerful to influence the preferred frequency. Our simulations support that the influence of ion channels on spike timing reliability also holds for more realistic rhythmic stimulus waveforms. Dynamic-clamp experiments in slices of rat prefrontal cortex confirm the theoretical prediction that slow potassium channels can mediate a change in spike timing reliability, dependent on the frequency of the input.

In the second part of the RESULTS section (*Influence of conductances on spike timing reliability at the preferred frequency*) we explore the influence of ion channels beyond changes in preferred frequency attributed to the resonance effect. Different neurons may have the same preferred frequency (i.e., the same DC firing rate) but different composition of ion channels. We analyze the influence of slow potassium channels and persistent sodium channels on spike timing reliability for neurons with the same preferred frequency. We find that both channel types significantly influence spike timing reliability. Slow potassium channels increase reliability, whereas persistent sodium channels lower it.

METHODS

Model cells

The single-compartment conductance-based model neurons were implemented in NEURON. In the basic implementation, the neurons contained fast sodium channels (Na), delayed-rectifier potassium channels (K_{dr}), leak channels (leak), slow potassium channels (K_s), and persistent sodium channels (Na_P). The time resolution of the numerical simulation was 0.1 ms. The kinetic parameters of the 5 basic channel types and reversal potentials were taken from a model of a cortical pyramidal cell Golomb and Amitai (1997), apart from the reversal potential of the leak

channels, which was set to −80 mV (to avoid spikes in the absence of input and noise). The conductances of the cell we will refer to as the *reference cell* were (in mS/cm^2): g_{Na} = 24, g_{Kdr} = 3, g_{leak} = 0.02, g_{Ks} = 1, and g_{NaP} = 0.07 (Golomb and Amitai 1997). Its input resistance was 186 MΩ. The slow potassium conductance represented potassium channels with an activation time on the order of several tens to hundreds of milliseconds (here 75 ms). In the model it is responsible for a spike frequency adaptation to a current step, which is experimentally observed in cortical pyramidal neurons (Connors and Gutnick 1990; McCormick et al. 1985). We also investigated cells where the K_s channels were replaced by muscarinic potassium channels (K_M) and by calcium-dependent potassium channels (K_{Ca}). The muscarinic channel K_M was a slow noninactivating potassium channel with Hodgkin–Huxley style kinetics (Barkai et al. 1994; Storm 1990). The calcium-dependent conductance K_{Ca} was based on first-order kinetics and was responsible for a slow afterhyperpolarization (Tanabe et al. 1998). This channel was activated by intracellular calcium and did not depend on voltage. Because of the dependency of K_{Ca} on calcium, we also inserted an L-type calcium channel as well as a simple Ca-ATPase pump and internal buffering of calcium. For the parameters of these additional currents see APPENDIX. Kinetic parameters of all channels used were set to 36°C.

Stimulus waveforms

The stimuli used to characterize spike timing reliability of individual cells consisted of 2 components. The first component was a constant depolarizing current I_{DC}, which was the same for all model cells (apart from the simulations designed to study of the influence of the DC), and which also remained fixed throughout experimental recording of a cell. The second component was a sine wave with frequency f

$$i(t)=C\sin[2\pi ft]+I_{DC}$$

The amplitude of the sine wave C was always smaller than I_{DC}. Examples of stimuli are shown in Fig. 1, *B* and *C*.

To characterize spike timing reliability in model cells, we applied a set of such stimuli with 70 different frequencies (1–70 Hz in 1-Hz increments) and 3 different amplitudes of the sine wave component (C = 0.05, 0.1, and 0.15 nA). I_{DC} = 0.3 nA in all cases. For each frequency and amplitude combination, spikes for n = 20 repeated trials of the same stimulus (duration 2.0 s) were recorded. Reliability was calculated based on spiking responses 500 ms after the onset of the stimulus, discarding the initial transient. To simulate intrinsic noise, we also injected a different random zero-mean noise of small amplitude [SD σ = 20 pA] on each individual trial. For the reference cell the noise resulted in voltage fluctuations of about 1.3 mV SD at rest. The noise was generated from a Gaussian distribution and filtered with an alpha function with a time constant of τ = 3 ms. Although overall reliability systematically decreased with the size of the noise, neither the frequency content of the noise nor the absolute size of the noise (in that range) significantly changed the results. Spike times were determined as the time when the voltage crossed −20 mV from below. The input resistance for the model cells was estimated by application of a depolarizing DC current step sufficiently large to depolarize the cell by ≥10 mV.

Model neurons were also tested with a stimulus where power was distributed around one dominant frequency. These more realistic stimuli were constructed to have a peak in the power spectrum in either the theta- or the gamma-frequency range. These waveforms mimic theta- and gamma-type inputs and were created by inverse Fourier transform of the power spectrum (with random phases). For the theta-rich wave, the power spectrum consisted of a large peak

at 8 Hz (Gaussian, σ = 1 Hz) and a small peak at 50 Hz (Gaussian, σ = 6 Hz). For gamma-rich waves, the power spectrum had a large peak at 30 or 50 Hz (with σ = 3 and 6 Hz, respectively), and a small peak at 8 Hz (σ = 1 Hz). These waveforms were first normalized to have a root-mean-square (RMS) value of 1 and were then used with different scaling factors (yielding different RMS values). The DC component was added after scaling. These stimuli were presented for 10 s and when evaluating reliability, the first 500 ms after stimulus onset were discarded.

The reliability measure

Spike timing reliability was calculated from the neuronal responses to repeated presentations of the same stimulus. For the model studies this implied the same initial conditions, but different noise for each trial. Reliability was quantified by a correlation-based measure, which relies on the structure of individual trials and does not require the definition of a priori events. For a more detailed discussion of the method see Schreiber et al. (2003). The spike trains obtained from N repeated presentations of the same stimulus were smoothed with a Gaussian filter of width $2\sigma_t$, and then pairwise correlated. The normalized value of the correlation was averaged over all pairs. The correlation measure R_{corr}, based on the smoothed spike trains, $\vec{s}_i$ (i = 1, …, N), is

$$R_{\text{corr}} = \frac{2}{N(N-1)} \sum_{i=1}^{N} \sum_{j=i+1}^{N} \frac{\vec{s}_i \cdot \vec{s}_j}{|\vec{s}_i||\vec{s}_j|}$$

The normalization guarantees that $R_{\text{corr}} \in [0; 1]$. R_{corr} = 1 indicates the highest reliability and R_{corr} = 0 the lowest. For all model cell studies, σ_t = 1.8 ms and for the experimental data σ_t = 3 ms. The value of σ_t for model cells was chosen such that, given the noise level, reliability values R_{corr} exploited the possible range of its values [0; 1], allowing for better discrimination between reliable and unreliable spike timing. The experimental data proved more noisy and therefore a larger σ_t was chosen to yield a good distinction between reliable and unreliable states. All evaluation of model and experimental data (beyond obtaining spike times) was performed in Matlab.

Firing rate analysis

For the firing rate analysis, the full parameter space of Na, Na_P, K_{dr}, K_s, and leak conductances was analyzed. DC firing rates were obtained for all possible parameter combinations within the parameter space of the 5 conductances considered (see APPENDIX). The maximum change in firing rate achievable by one ion channel type was characterized (for each combination of the other 4 conductances) as the difference between the maximum and minimum (nonzero) firing rates achievable by variation of the ion channel conductance of interest, keeping the other 4 conductances fixed. If a cell never fired despite variation in one conductance, it was excluded from the parameter space (<5% of the total 4-dimensional conductance space for any channel type tested). The distribution of maximum changes in firing rate achievable by variation of the density of one ion channel type over all combinations of the other 4 densities is presented in the paper.

Experimental protocols

Coronal slices of rat prelimbic and infra limbic areas of prefrontal cortex were obtained from 2- to 4-wk-old Sprague-Dawley rats. Rats were anesthetized with Isoflurane (Abbott Laboratories, North Chicago, IL) and decapitated. Brains were removed and cut into 350-μm-thick slices using standard techniques. Patch-clamp was performed under visual control at 30–

32°C. In most experiments Lucifer yellow (RBI, 0.4%) or Biocytin (Sigma, 0.5%) was added to the internal solution. In all experiments, synaptic transmission was blocked by D-2-amino-5-phosphonovaleric acid (D-APV; 50 μM), 6,7-dinitroqui-noxaline-2,3, dione (DNQX; 10 μM), and biccuculine methiodide (Bicc; 20 μM). All drugs were obtained from RBI or Sigma, freshly prepared in artificial cerebrospinal fluid, and bath applied. Whole cell patch-clamp recordings were achieved using glass electrodes (4–10 MΩ) containing (in mM): $KMeSO_4$, 140; Hepes, 10; NaCl, 4; EGTA, 0.1; MgATP, 4; MgGTP, 0.3; phosphocreatine, 14. Data were acquired in current-clamp mode using an Axoclamp 2A amplifier (Axon Instruments, Foster City, CA).

Data were acquired using 2 computers. The first computer was used for standard data acquisition and current injection. Programs were written using Labview 6.1 (National Instrument, Austin, TX) and data were acquired with a PCI16E1 data acquisition board (National Instrument). Data acquisition rate was either 10 or 20 kHz. The second computer was dedicated to dynamic clamp. Programs were written using either a Labview RT 5.1 (National Instrument) or a Dapview (Microstar Laboratory, Bellevue, WA) frontend and a C language backend. Dynamic clamp (Hughes et al. 1998; Jaeger and Bower 1999; Sharp et al. 1993) was implemented using a DAP5216a board (Microstar Laboratory) at a rate of 10 kHz. A dynamic clamp was achieved by implementing a rapid (0.1-ms) acquisition/injection loop in current-clamp mode. All experiments were carried in accordance with animal protocols approved by the N.I.H.

Stimuli consisted of sine waves of 30 different frequencies (1–30 Hz) presented for 2 s. Only one amplitude was tested. No additional noise was injected. The first 500 ms were discarded for analysis of reliability.

RESULTS

Spike timing reliability of conductance-based model neurons was characterized using a sine wave stimulation protocol for model cells with different amounts of sodium, potassium, and leak conductances. The voltage response of the reference model cell (see METHODS) to stimulation with a DC step current (I_{DC} = 0.3 nA) is shown in Fig. 1*A*.

Model cells were stimulated with a set of sine waves on top of a fixed DC. Reliability values for each individual stimulus and cell, based on correlation of responses to repeated presentation of a stimulus each with an independent realization of the noise, were derived as a function of the frequency *f* and the amplitude of the sine component *C*. Figure 1, *B–E* show examples of 2 stimuli used and responses to those stimuli obtained from the reference cell. Figure 1*F* shows the complete set of reliability values as a function of frequency and amplitude of the sine component of the input.

Distinct, tongue-shaped regions of high reliability, so-called Arnold tongues (Beierholm et al. 2001), arising from the resonance effect of spike timing reliability, are visible. Figure 1*F* also shows that the degree of reliability depended on the power of the input at the resonant frequency of a neuron. The higher the amplitude at the resonant frequency, the more pronounced was the reliability. At high amplitudes, frequencies close to the resonant frequency also showed enhanced reliability. The Arnold tongues were approximately vertical, so that the frequency of maximum reliability showed only a weak dependency on the amplitude of the sine component. The difference in input frequency for maximal reliability, as the amplitude *C* varied from 0.05 to 0.15 nA, was usually <2 Hz. In most examples presented in this study, the strongest resonance was found at a 1:1 locking to the stimulus, where one spike per cycle of the sine wave was elicited. Additional regions of enhanced reliability could be observed at harmonics of the main resonant frequency (1:2, 1:3, and 1:4 phase locking, in order of decreasing strength), and at the 1st subharmonic (2:1 phase locking).

The location of the strongest Arnold tongue in frequency space revealed the preferred frequency of a neuron, which was well approximated by the firing rate of the neuron in response to the DC component alone. Figure 1*G* shows a strong correlation between the preferred frequency (i.e., position of the strongest Arnold tongue on the frequency axis determined by the frequency of highest reliability for a given amplitude, *C*) and the DC firing rate of a cell for a wide range of conductance values in the model (see APPENDIX). In all (but 2) cases the resonant frequency was close to the DC firing rate. Usually, the resonant frequency at the lowest amplitude of the sine component was closest to the DC firing frequency. For the 2 outliers the highest value of reliability was achieved at the subharmonic, or the 1st harmonic of the DC firing frequency. The importance of the DC firing rate in generating phase-locked firing patterns was previously emphasized (see e.g. Coombes and Bressloff 1999; Hunter et al. 1998; Keener et al. 1981; Knight 1972; Rescigno et al. 1970). The resonant frequency is referred to as *preferred frequency* throughout the paper.

Influence of conductances on the frequency preference

Because ionic conductances are known to influence neuronal activity levels, we investigated the ability of ion channels to modulate the preferred frequency in the first part of this study.

SIMULATION RESULTS FOR A CORTICAL SINGLE-COMPARTMENT MODEL CELL—We started from the model of a cortical neuron (the reference cell). First, we varied one channel density at a time, keeping the densities of the other channels fixed. The Arnold plots of cells whose leak density and slow potassium density were varied respectively are shown in Fig. 2. Example spike shapes (at DC stimulation) are shown next to the Arnold plots.

All cells showed a pronounced resonance—that is, a pronounced preferred frequency. For variation of the leak channels, the preferred frequency shifted to slightly lower frequencies with increasing density of leak channels. In contrast to variation in leak channels, variation of K_s conductance showed a large shift in preferred frequency (see Fig. 2*B*). We also explored changes in preferred frequency induced by the other conductances (i.e., Na, K_{dr}, and Na_P). Preferred frequencies yielding maximum reliability (at $C = 0.1$ nA) as a function of normalized channel density are shown in Fig. 3 for all channels, including leak and K_s.

Because each channel type operated in a different range of densities, some of which differed by orders of magnitude, we normalized (for parameter range criteria see APPENDIX) the densities to the range [0; 1] for each channel type, respectively. For Na, K_{dr}, and Na_P large changes in densities were necessary to shift the preferred frequency. The overall observed change for these channel types was in the range of 5 to 15 Hz. Thus starting from the reference cell, only variation in the K_s density could shift the preferred frequency by several tens of Hertz, from <10 to >60 Hz.

In all cases studied, for a given channel density the reliability at the preferred frequency was also higher than it would have been at this stimulus frequency for most other values of channel densities. Comparably high values were achieved only for channel densities where the frequency at the 1st harmonic or the subharmonic Arnold tongue coincided with the stimulus frequency.

We also analyzed the influence of 2 other potassium channels with slower kinetics on frequency preference of the reference cell—a muscarinic potassium channel K_M and a calcium-dependent potassium channel K_{Ca} (for details see APPENDIX). For both cases, we substituted K_s by the new potassium conductance, K_M or K_{Ca}, respectively. The results of the Arnold plot analysis are shown in Fig. 3*B*. For both channel types, an increase of their conductance shifted the preferred frequency over a broad range of frequencies. The lowest achievable frequency at a given DC depended on the time constant of the slow potassium conductance. If 2 or more slow

potassium conductances were present at high densities, the broad tuning effect was diminished and eventually suppressed at high conductance levels (data not shown). Figure 3*C* presents the preferred frequency as a function of K_s conductance for different τ_{Ks}. The slower the kinetics of the K_s channel, the lower the minimum achievable frequency and the broader the frequency range accessible through variation of the slow potassium conductance.

For completeness we analyzed all combinations of Na, Na_P, K_{dr}, K_s, and leak conductances. In this case, we relied on the DC firing rate as an estimate of the preferred frequency. The distribution of maximum changes in firing rate (i.e., preferred frequency) achievable by variation of the density of one ion channel type over all combinations of the other 4 densities is presented in Fig. 4, which shows one curve for each ion channel type. For a more detailed description of this analysis see METHODS. Variation of K_s had a significant effect on the firing frequency in almost all parameter regimes. Its influence was weakest when another potassium channel, K_{dr} in this case, was present at high density. The mean change achieved with K_s was around 20 Hz. The mean change achieved by the other ion channels was <10 Hz.

The analysis also showed that, in principle, all ion channel types could achieve firing rate changes of ≥20 Hz. Within the parameter space investigated, this was true for only a minority of values of the other 4 conductances. Figure 4*B* shows 4 examples of parameter regimes where these channels significantly changed the preferred frequency. For example, this occurred for K_{dr} when K_s was not present or present only in small amounts. Na_P could cause a large frequency shift when both potassium conductances, K_{dr} and K_s, were low. Na was potent in changing the frequency when both potassium conductances and Na_P were low. Its influence in these cases weakened further with a higher density of leak channels. Leak channel variation also gave rise to higher frequency shifts when both potassium conductances were low and the sodium conductances were not too large. In general, higher densities of leak channels tended to lower the minimum achievable frequency.

To illustrate that regulation of ionic conductances on spike timing reliability frequency preference would allow a cell to dynamically adjust its spike timing reliability, the effect of a temporary increase in K_s conductance on spike timing reliability is presented in Fig. 5. The conductance step was chosen such that the preferred frequency of the cell after the conductance increase matched the stimulus frequency. Spike timing reliability during elevation of the K_s conductance was significantly enhanced.

RELIABILITY OF INPUTS WITH MORE THAN ONE FREQUENCY—Many biologically relevant periodic inputs, such as inputs to neurons that participate in rhythms, exhibit a broad distribution of frequencies in their power spectrum. We therefore stimulated model neurons with quasi-random stimuli whose power spectrum contained 2 peaks, one in the theta-range (about 8 Hz) and one in the gamma range (30–70 Hz). The 3 rhythm-like stimuli tested are depicted in Fig. 6.

The reliability of a response to one of those stimuli depended on the amount of K_s present in the neuron. For the theta-dominated input (Fig. 6*A*) cells with higher K_s conductances responded more reliably, whereas cells with lower K_s conductance (therefore tuned to higher frequencies) responded with lower reliability. For the gamma-dominated input, only cells with an optimally low K_s conductance achieved a high reliability. A high K_s conductance made the cell more unreliable. For all stimuli, the cell with preferred frequency (adjusted by K_s) closest to the dominant frequency in the input yielded the highest spike timing reliability (as illustrated by the *lower panels* in Fig. 6). Interestingly, the second (smaller) peak in the power spectra of the inputs was also reflected by a small increase of reliability at corresponding densities of K_s. Not surprisingly, reliability also tended to increase with the variance (or RMS value), of the stimuli, across all stimuli and cells.

EXPERIMENTAL RESULTS—To test the effects of slow potassium channels on preferred frequency physiologically, we performed patch-clamp recordings in slices of rat prefrontal cortex. We used the dynamic-clamp technique, which allows time-dependent currents to be injected that experimentally simulate conductances through on-line feedback. Thus we were able to artificially introduce K_s currents (with the same dynamics as the K_s reference channel used in the model simulations above). We first characterized its spike timing reliability as a function of frequency of a sine wave input in the "native" conductance state of the cell (the control state). Then we recorded responses to the same set of stimuli, in the presence of an additional K_s conductance in the cell, which was introduced with dynamic clamp (the K_s state). The DC level was kept constant and was the same for the control and the K_s experiment. Figure 7 shows spike timing reliability as a function of the frequency of the input for the control and K_s states. In the control experiment the cell had a preferred frequency at about 17 Hz. When K_s was introduced, the preferred frequency was lowered to 7 Hz and the spike timing reliability was increased beyond the maximum reliability of the control state. We observed a negative shift in the preferred frequency for all cells recorded (n = 4). For most cells, the shift in the preferred frequency resulted in an increase of spike timing reliability at that value (n = 3).

Influence of conductances on spike timing reliability at the preferred frequency

Our analysis supports that changes in ionic conductance can mediate changes in the preferred frequency through variation of the firing rate. However, we also found an effect of individual conductances on spike timing reliability not involving changes of the preferred frequency. We show that the overall level of reliability at the preferred frequency also depends on individual conductances, in addition to the general frequency preference discussed in the first part.

We created a set of cells with the same preferred frequency (at I_{DC} = 0.3 nA), but different time constants of the K_s channel. The peak conductance g_{Ks} of each cell was adjusted such that the DC firing rate (i.e., preferred frequency) amounted to 20 Hz. All other conductance parameters were those of the reference cell. Sine wave stimulation of these cells confirmed that cells within one set had the same preferred frequency (Fig. 8*A*).

However, there was a systematic difference in the value of reliability at the preferred frequency, in the width of the 1:1 Arnold tongue, as well as in the values of spike timing reliability at the harmonic frequencies (1:2 and 1:3 Arnold tongues). The absolute value of reliability at the preferred frequency and its harmonics increased significantly with decreasing τ_{Ks} [i.e., faster kinetics and higher values of g_{Ks}, Fig. 8, *C* and *D*]. This effect was more pronounced at the 1st harmonic of the preferred frequency, despite a small deviation from the general trend around τ_{Ks} = 25 ms. The width also increased with faster kinetics and larger values of g_{Ks}. Figure 8, *F* and *G* show the voltage traces at the 1st harmonic for τ_{Ks} values of 10 and 150 ms. The increase in reliability with larger and faster K_s conductance was accompanied by a deepening of the afterhyperpolarization following a spike (see Fig. 8) and a more efficient shutdown of sodium currents after a spike (not shown).

To distinguish the contribution of the peak conductance and the time constant of the slow potassium channel in this observation, 2 separate sets of neurons with a preferred frequency of 20 Hz were created. Cells in the 1st set varied in the K_s peak conductance. This time, the DC was adjusted to keep the firing rate at 20 Hz. Cells in the 2nd set differed in the time constant τ_{Ks}. Again, adjustment of the DC kept the firing rate constant. The amplitude of the sine wave component of the input was the same for all cells.

Figure 9*A* shows a significant influence of K_s peak conductance on reliability at the preferred frequency for all 3 amplitude levels tested. Also, the width of the reliable region around the preferred frequency increased with g_{Ks} (Fig. 9*D*). For low conductance values, the curves were nonmonotonic. For these values, the difference between the peak reliability and that at

surrounding frequencies was very small, which as a consequence broadened the estimate of width at the preferred frequency. The time constants also influenced spike timing reliability at the preferred frequency. Apart from a shallow maximum around τ_{Ks} = 30 ms, the general trend confirmed that faster K_s channels increase the peak reliability and broaden the width. Overall, the effect of the K_s peak conductance was higher than that of the time constant.

Our analysis supports the hypothesis that a higher slow potassium peak conductance and faster potassium kinetics promote spike timing reliability. We also found that the persistent sodium channel Na_P decreased spike timing reliability. Figure 9*C* illustrates the finding for a set of cells with different amounts of Na_P peak conductance and adjusted DC (to yield a preferred frequency of 20 Hz). The higher the Na_P peak conductance, the lower was the peak value of reliability. Even more significant was the effect of Na_P on the width of the 1:1 Arnold tongue. The more Na_P was present, the narrower was the band of increased reliability around the preferred frequency.

DISCUSSION

We have explored the influence of intrinsic cell properties on spike timing reliability. Conductance-based models of cortical neurons were used to demonstrate 2 functional aspects by which ion channels can influence spike timing reliability. The first aspect concerns the setting of the frequency preference for spike timing reliability. The second aspect concerns the influence of ion channel kinetics and density on spike timing reliability not involving changes in preferred frequency (i.e., for the same overall excitability).

We first showed that neurons exhibit a preferred frequency for spike timing reliability, which correlates with the DC firing rate and can be regulated at the level of ion channels. Reliability is increased around the preferred frequency, but also around the harmonics and subharmonics of the preferred frequency. These findings confirm the resonance effect described by Hunter et al. (1998) in models of leaky integrate-and-fire neurons and in recordings from *Aplysia* motoneurons. We analyzed the influence of conductances in cortical cells and provided numerical and experimental support that slow potassium channels can regulate the preferred frequency. We showed that conductance-based regulation of reliability also extends to more realistic rhythm-like inputs that contain more than one frequency.

In a second step we studied the influence of ionic conductances and their kinetics on spike timing reliability beyond the location of the resonance effect of spike timing reliability in frequency space. We compared cells of the same DC firing rate and found that more and faster slow potassium channels enhance absolute reliability levels at the preferred frequency, whereas persistent sodium channels impair reliability.

Adjustment of preferred frequency through potassium channels

Analysis of pyramidal model neurons has revealed that the slow potassium conductance has a significant potential to tune the preferred frequency for spike timing reliability. Potassium currents counteract depolarization and set a limit to overall excitability. Controlling the interspike interval during repetitive firing (Hille 2001), they set the firing rate and thus preferred frequency. This observation was confirmed for a general model of a K_s channel, as well as a muscarinic potassium channel (K_M) and a calcium-dependent potassium channel (K_{Ca}). Furthermore, we saw that the range of achievable firing rates through variation in K_s depended on the time constant of the channel. The faster the channel, the smaller the range of possible preferred frequencies.

Given the relation between preferred frequency and firing rate, it is not surprising that the other conductances are important too. First, they determine the DC firing rate if no slow potassium

channels are present and thus set the upper limit of preferred frequencies that can be achieved by adjustment of K_s. Second, sodium leak and faster potassium channels also mediate larger shifts in frequency. Generally, the other channels extended their influence on preferred frequency with decreasing K_s conductance. The presence of (at least one) large potassium conductance, on the contrary, tended to dominate excitability, slower channels being more effective. Along those lines, the influence of K_s itself was weakest when the delayed rectifier conductance K_{dr} was strong (data not shown).

Pyramidal neurons in cortex show a strong adaptation, presumably mediated by a slow potassium conductance. Therefore we conclude that in these cells, the slow potassium conductance can efficiently regulate the spike timing reliability frequency preference. The firing rate analysis, however, depends on the parameter range of the pyramidal cell model. The experiments in slices of rat prefrontal cortex support the potential of the slow potassium conductance to shift frequency preference.

Potassium channels improve spike timing beyond a shift in preferred frequency

Analyzing neurons of the same preferred frequency but different K_s densities and kinetics revealed that ionic conductances can increase or decrease spike timing reliability without involving changes in overall excitability and preferred frequency. The effect was most pronounced at the preferred frequency and its harmonics. However, we also analyzed reliability in response to the DC alone and found a small effect. For a pure DC input, phase locking is not possible because the only time-varying signal is the noise, which is different in each trial and therefore randomizes spike timing for large times after stimulus onset. Nevertheless, spike timing reliability during the 1st second after stimulus onset (not counting the initial 500 ms) was significantly more precise for neurons with the higher and faster K_s conductance (data not shown). This suggests that the improvement of reliability with more and faster K_s channels results from a reduced sensitivity to noise after a spike. The deepening of the afterhyperpolarization and the more efficient shut down of sodium channels observed after a spike support this hypothesis. The separation of the effects of K_s time constant and K_s peak conductance showed that both parameters influence spike timing reliability, although the effect of peak conductance seemed somewhat more dominant. Variation of the time constant seemed to exhibit a small nonmonotonic influence on reliability for lower values, which will be subject to further investigation.

Potassium channels are promising candidates for regulating both the preferred frequency and the reliability at the preferred frequency. The trends for tunable frequency range (slower K_s channels are better) and the value of reliability at the preferred frequency (faster K_s channels are better) are opposed. Indeed, potassium channels are the ion channels with the greatest diversity, with gating kinetics that span several orders of magnitude (Hille 2001). They are regulated by a multitude of cellular signals and neuromodulators, examples of which are cAMP-dependent phosphorylation of slow potassium channels in the heart or regulation of muscarinic potassium channels through acetylcholine.

Functional importance of reliability modulation

In principle, the frequency tuning of spike timing reliability may be important for cells that are stimulated by inputs with dominant frequencies that do not change with time, such as frequency-tuned cells at the periphery of the auditory system. Differential expression of channel densities and different types of ion channels to match the prevalent input frequencies is not unknown, although it has not yet been shown to regulate spike timing reliability. One example for a different mechanism is the gradient of calcium and potassium channels in cochlear hair cells of lower vertebrates, which support electrical tuning to sound pressure waves of particular frequencies (Hille 2001). In addition, cells could in principle also regulate spike

timing reliability dynamically. Important central signals are, for example, hippocampal, theta and gamma rhythms. There, cells may change their spike timing frequency preference through cellular messengers or neuromodulators on relatively short time scales. As our examples of more rhythm-like inputs suggest (Fig. 6), adjustment of spike timing frequency preference can also increase reliability for more natural types of inputs, such as theta- or gamma-type oscillations.

Future directions

Because the preferred frequency correlates with the DC firing rate of a cell, the preferred frequency does not only depend on intrinsic properties of a cell, but also on the DC level of the input, or in other words, the mean level of depolarization, as a recent study of Hunter and Milton (2003) has shown. Thus intrinsic spike timing preferences depend on the signal mean as well as synaptic input, reflecting the interplay between intrinsic properties and properties of the network. However, extrinsic changes of the DC such as modification of synaptic inputs can influence the value of the preferred frequency only according to the status of the intrinsic parameters of a cell. Changes of reliability at the preferred frequency cannot be achieved without tuning of intrinsic properties of a cell.

A recent investigation has shown that the intrinsic currents determine the state of synchrony in neural networks (Pfeuty et al. 2003). When the network is in a synchronous state and each neuron receives periodic input, an individual neuron in the network maintains synchrony by phase locking, which produces reliable spike timing. Interestingly, the results of Pfeuty et al. (2003) indicate that slow potassium currents promote synchrony in a network of conductance-based neurons, whereas persistent sodium channels impede it, which is in accordance with our findings of the influence of these channels on spike timing reliability. They also point out that synchrony varies with the firing rate depending on the intrinsic currents, which may be attributed to a resonance effect of synchrony, similar to that of spike timing reliability.

An aspect that we did not explore in the analysis is the possibility that channels may be regulated together, as a recent study of MacLean and colleagues (2003) has shown. If more than one channel type is regulated together (by gene expression or neuromodulation), a more efficient combination of conductances could be obtained.

The signals that we analyzed are suprathreshold mean signals. For lower levels of depolarization (signals with sub-threshold mean) the prediction of the preferred frequency through the DC firing fails. It is probable that in this regime other intrinsic properties of cells, for instance determined by conductances that are activated at lower levels of depolarization, may shape spike timing frequency preferences of neurons. Channels like I_H or I_{KA}, which do not significantly influence suprathreshold signals (data not shown), are likely to gain importance.

In conclusion, regulation of conductances of a cell can efficiently affect spike timing reliability for inputs with dominant frequencies and suprathreshold mean. Changes in conductances can therefore be exploited to adjust spike timing reliability to the dominant input frequency. Moreover, ion channels also can influence spike timing reliability without changes to the mean firing rate. Spike timing reliability is the result of several mechanisms (of intrinsic and network origin), including the mean level of depolarization (Hunter and Milton 2003), which may be regulated through the background synaptic input, or well timed inhibitory or excitatory input (see e.g. Mehta et al. 2002).

Acknowledgments

We thank I. Samengo for valuable discussions and detailed comments on the manuscript.

GRANTS

This work was supported by the Daimler-Benz Foundation, the Sloan-Swartz Center for Theoretical Neurobiology, the German National Merit Foundation, and the Howard Hughes Medical Institute.

References

Barkai E, Bergman RE, Horwitz G, Hasselmo ME. Modulation of associative memory function in a biophysical simulation of rat piriform cortex. J Neurophysiol 1994;72:659–677. [PubMed: 7527075]

Beierholm U, Nielsen CD, Ryge J, Alstrom P, Kiehn O. Characterization of reliability of spike timing in spinal interneurons during oscillating inputs. J Neurophysiol 2001;86:1858–1868. [PubMed: 11600645]

Brette R, Guigon E. Reliability of spike timing is a general property of spiking model neurons. Neural Comput 2003;15:279–308. [PubMed: 12590808]

Connors B, Gutnick M. Intrinsic firing patterns of diverse neocortical neurons. Trends Neurosci 1990;13:365–366. [PubMed: 1699324]

Coombes S, Bressloff PC. Mode locking and Arnold tongues in integrate-and-fire neural oscillators. Phys Rev E Stat Phys Plasmas Fluids Relat Interdiscip Top 1999;60:2086–2096.

Destexhe A, Babloyantz A, Sejnowski TJ. Ionic mechanisms for intrinsic slow: oscillations in thalamic relay neurons. Biophys J 1993;65:1538–1552. [PubMed: 8274647]

Destexhe A, Contreras D, Sejnowski TJ. A model of spindle rhythmicity in the isolated thalamic reticular nucleus. J Neurophys 1994;72:803–818.

Fellous JM, Houweling AR, Modi RH, Rao RP, Tiesinga PH, Sejnowski TJ. Frequency dependence of spike timing reliability in cortical pyramidal cells and interneurons. J Neurophysiol 2001;85:1782–1787. [PubMed: 11287500]

Fricker D, Miles R. EPSP amplification and the precision of spike timing in hippocampal neurons. Neuron 2000;28:559–569. [PubMed: 11144364]

Goldman MS, Golowasch J, Marder E, Abbott LF. Global structure, robustness, and modulation of neuronal models. J Neurosci 2001;21:5229–5238. [PubMed: 11438598]

Golomb D, Amitai Y. Propagating neuronal discharges in neocortical slices: computational and experimental study. J Neurophysiol 1997;78:1199–1211. [PubMed: 9310412]

Gutfreund Y, Yarom Y, Segev I. Subthreshold ocsillations and resonant frequency in guinea pig cortical neurons - physiology and modeling. J Physiol 1995;483:621–640. [PubMed: 7776248]

Gutkin B, Ermentrout G, Rudolph M. Spike generating dynamics and the conditions for spike-time precision in cortical neurons. J Comput Neurosci 2003;15:91–103. [PubMed: 12843697]

Haas JS, White JA. Frequency selectivity of layer II stellate cells in the medial entorhinal cortex. J Neurophys 2002;88:2422–2429.

Hille, B. Ion Channels of Excitable Membranes. 3. Sunderland, MA: Sinauer Associates; 2001.

Hughes SW, Cope DW, Crunelli V. Dynamic clamp study of Ih modulation of burst firing and delta oscillations in thalamocortical neurons in vitro. Neuroscience 1998;87:541–550. [PubMed: 9758221]

Hunter JD, Milton G. Amplitude and frequency dependence of spike timing: implications for dynamic regulation. J Neurophysiol 2003;90:000–000.

Hunter JD, Milton JG, Thomas PJ, Cowan JD. Resonance effect for neural spike time reliability. J Neurophysiol 1998;80:1427–1438. [PubMed: 9744950]

Jaeger D, Bower JM. Synaptic control of spiking in cerebellar purkinje cells: dynamic current clamp based on model conductances. J Neurosci 1999;19:6090–6101. [PubMed: 10407045]

Jensen RV. Synchronization of randomly driven nonlinear oscillators. Phys Rev E Stat Phys Plasmas Fluids Relat Interdiscip Top 1998;58:6907–6910.

Keener J, Hoppensteadt F, Rinzel J. Integrate-and-fire models of nerve membrane response to oscillatory input. SIAM J Appl Math 1981;41:503–517.

Knight BW. The relationship between the firing rate of a single neuron and the level of activity in a population of neurons. Experimental evidence for resonant enhancement in the population response. J Gen Physiol 1972;59:767–778. [PubMed: 5025749]

MacLean JN, Zhang Y, Johnson BR, Harris-Warrick RM. Activity-independent homeostasis in rhythmically active neurons. Neuron 2003;37:109–120. [PubMed: 12526777]

Magee JC. A prominent role for intrinsic neuronal properties in temporal coding. Trends Neurosci 2002;26:14–16. [PubMed: 12495857]

Mainen Z, Sejnowski T. Reliability of spike timing in neocortical neurons. Science 1995;168:1503–1506. [PubMed: 7770778]

Mainen Z, Sejnowski T. Influence of dendritic structure on firing pattern in model neocortical neurons. Nature 1996;382:363–366. [PubMed: 8684467]

Marder E, Abbott LF, Turrigiano GG, Liu Z, Golowasch J. Memory from the dynamics of intrinsic membrane currents. Proc Natl Acad Sci USA 1996;93:13481–13486. [PubMed: 8942960]

McCormick D, Connors B, Lighthall J, Prince DA. Comparative electrophysiology of pyramidal and sparsely stellate neurons of the neocortex. J Neurophysiol 1985;54:782–805. [PubMed: 2999347]

Mehta MR, Lee AK, Wilson MA. Role of experience and oscillations in transforming a rate code into a temporal code. Nature 2002;417:741–746. [PubMed: 12066185]

Nowak LG, Sanchez-Vives MV, McCormick DA. Influence of low and high frequency inputs on spike timing in visual cortical neurons. Cereb Cortex 1997;7:487–501. [PubMed: 9276174]

Pfeuty B, Mato G, Golomb D, Hansel D. Electrical synapses and synchrony: The role of intrinsic currents. J Neurosci 2003;23:6280–6294. [PubMed: 12867513]

Reinagel P, Reid RC. Precise firing events are conserved across neurons. J Neurosci 2002;22:6837–6841. [PubMed: 12177180]

Rescigno A, Stein R, Purple R, Poppele R. A neuronal model for the discharge patterns produced by cyclic inputs. Bull Math Biophys 1970;32:337–353. [PubMed: 4327360]

Schreiber S, Fellous J-M, Whitmer D, Tiesinga PHE, Sejnowski T. A new correlation-based measure of spike timing reliability. Neurocomputing. 2003 in press.

Sharp AA, O'Neil MB, Abbott LF, Marder E. Dynamic clamp: computer-generated conductances in real neurons. J Neurophysiol 1993;69:992–995. [PubMed: 8463821]

Storm JF. Potassium currents in hippocampal pyramidal cells. Prog Brain Res 1990;83:161–187. [PubMed: 2203097]

Tanabe M, Gahwiler BH, Gerber U. L-type Ca^{2+} channels mediate the slow Ca^{2+}-dependent afterhyperpolarization current in rat CA3 pyramidal cells in vitro. J Neurophysiol 1998;80:2268–2273. [PubMed: 9819242]

Tiesinga PHE. Precision and reliability of periodically and quasiperiodically driven integrate-and-fire neurons. Phys Rev E Stat Phys Plasmas Fluids Relat Interdiscip Top 2002;65:041913.

Tiesinga PHE, Fellous J-M, Sejnowski TJ. Attractor reliability reveals deterministic structure in neuronal spike trains. Neural Comput 2002;14:1629–1650. [PubMed: 12079549]

Turrigiano G, Abbott LF, Marder E. Activity-dependent changes in the intrinsic properties of cultured neurons. Science 1994;264:974–977. [PubMed: 8178157]

Yamada Y, Nakazato Y, Ohga A. Ouabain distinguishes between nicotinic and muscarinic receptor-mediated catecholamine secretions in perfused adrenal-glands of cat. Br J Pharmacol 1989;96:470–479. [PubMed: 2924087]

APPENDIX

Conductance values

Table A1 summarizes the conductance values underlying the normalized conductances (Fig. 3). The second column states the parameter values used for the firing rate analysis (Fig. 4*A*).

TABLE A1

Summary of conductance values

	$\bar{g}$ for normalized conductances (mS/cm^2)	$\bar{g}$ for firing rate analysis (mS/cm^2)
$\bar{g}_{Na}$	(10, 15, 30, 50, 70, 100)	(1, 2, 3, …, 10) · 10
$\bar{g}_{NaP}$	(0, 0.07, 0.2, 0.3, 0.4)	(0, 1, 2, …, 10) · 0.04
$\bar{g}_{leak}$	(0, 0.005, 0.01, 0.015, 0.02, 0.025, 0.03, 0.035, 0.04)	(0, 1, 2, 3, 4) · 0.01
$\bar{g}_{Ks}$	(0.05, 0.1, 0.15, 0.2, 0.3, 0.4, 0.6, 1.0, 1.5, 2.0)	(0, 1, 2, …, 10) · 0.2
$\bar{g}_{Kdr}$	(1.5, 2, 3, 6, 10, 15, 20, 25, 30)	(1, 2, 3, …, 10) · 3
$\bar{g}_{M}$	(0.05, 0.1, 0.15, 0.2, 0.25, 0.3, 0.35, 0.4)	not used
$\bar{g}_{Kca}$	(0.02, 0.03, 0.04, 0.05, 0.07, 0.1, 0.2, 0.4, 0.5)	not used

The conductance values were chosen such that conductance changes from the reference cell resulted in regular spiking responses to I_{DC} = 0.3 nA, where the peak voltage of spikes was <50 mV, and no bursting was observed. We did not increase any conductance by more than a factor of 10 from the reference level. The conductance parameters of the 4 examples shown in Fig. 4*B* are given in Table A2.

TABLE A2

Summary of conductance values for the panels in Fig. 4B

	$\bar{g}_{Na}$ (mS/cm^2)	$\bar{g}_{NaP}$ (mS/cm^2)	$\bar{g}_{leak}$ (mS/cm^2)	$\bar{g}_{Ks}$ (mS/cm^2)	$\bar{g}_{Kdr}$ (mS/cm^2)
Na varied	varied	0	0.01	0.4	3
Na_P varied	30	varied	0.03	0.4	6
leak varied	20	0.04	varied	0.2	6
K_{dr} varied	40	0.08	0.03	0.2	varied

Additional channel kinetics

For most channels (Na, Na_P, K_{leak}, K_s, and K_{dr}) the details are given in the work of Golomb and Amitai (1997). The details of the K_M and channels K_{Ca} are given here.

The slow, noninactivating muscarinic potassium current K_M was defined as

$$I_M = \bar{g}_M n(V - E_K)$$
$$\frac{dn}{dt} = (n_\infty - n)/\tau_n$$
$$n_\infty = \{1 + \exp[-(V - \theta_n)/\sigma_n]\}^{-1}$$
$$\tau_n = 1,000\langle 3.3\{\exp[(V - \theta_{\tau_n})/\sigma_{1\tau_n}] + \exp[-(V - \theta_{\tau_n})/\sigma_{2\tau_n}]\}\rangle^{-1}/T_{adj}$$
$$T_{adj} = 3.0^{(T-22^\circ C)/10^\circ C}$$

where g_M is the peak muscarinic conductance, E_K = −90 mV, θ_n = − 35 mV, σ_n = 10 mV, θ_{τ_n} = −35 mV, $\sigma_{1\tau_n}$ = 40 mV, $\sigma_{2\tau_n}$ = 20 mV, and T = 36°C (cf. Gutfreund et al. 1995; Yamada et al. 1989). Values of τ_n < 0.001 were set to 0.001. Exponentials with arguments larger than 50 were set to exp(50).

The calcium-dependent potassium current K_{ca} was a nonvoltage-dependent potassium channel, activated by intracellular calcium. It was based on a first-order kinetic scheme

$$I_{Kca} = \bar{g}_{Kca} m^2 (V - E_K)$$
$$\frac{dm}{dt} = (m_\infty - m)/\tau_M$$
$$T_{adj} = 3.0^{(T-22^\circ C)/10^\circ C}$$
$$m_\infty = \frac{[Ca]_i^2}{\theta_{Kca}^2 + [Ca]_i^2}$$
$$\tau_M = \{\beta_M(1 + ([Ca]_i/\theta_{Kca})^2)\}^{-1}/T_{adj}$$

where $[Ca]_{i0}$ = 2.4e-04 mM (initial intracellular calcium concentration), β_M = 0.03 Hz (backward rate constant), θ_{Kca} = 5.0e-04 mM (midactivation concentration), T = 36°C [for reference also see Destexhe et al. (1994)]. If τ_M < 0.1 ms, then τ_M was set to 0.1 ms.

The functionality of K_{ca} requires intracellular calcium, whose dynamics include pumping of calcium ions and internal buffering, as well as a (voltage-dependent) calcium channel, Ca_L. We chose an L-type calcium channel with the following dynamics

$$I_{ca} = \bar{g}_{ca} u^2 z(V - E_{ca})$$
$$E_{ca} = 12.5\ mV \log([Ca]_o/[Ca]_i)$$
$$\frac{du}{dt} = (u_\infty - u)/\tau_u$$
$$\frac{dz}{dt} = (z_\infty - z)/\tau_z$$
$$V_x = -0.031(V + 37.1\ mV)$$
$$V_u = V + 24.6\ mV + c_u$$
$$V_z = V + 12.6\ mV + c_z$$
$$u_\infty = \{1 + \exp[-(V_u/\sigma_u)]\}^{-1}$$
$$\tau_u = 2.5\ ms[\exp(V_x/\sigma_x) + \exp(-V_x/\sigma_x)]^{-1}$$
$$z_\infty = [1 + \exp(V_z/\sigma_z)]^{-1}$$

where $\bar{g}_{ca}$ = 0.1 mS/cm^2 (maximum conductance of Ca_L), τ_z = 5,040 ms, σ_x = 1 mV, σ_u = 11.3 mV, σ_z = 18.9 mV. If abs (V_u) < 1e-04 mV then c_u was set to c_u = 0.00001 mV; otherwise c_u = 0 mV. If $abs(V_z)$ < 1e-04 mV then c_z was set to c_z = 0.00001 mV; otherwise c_z =0 mV.

The removal of intracellular calcium dynamics was accomplished by an ATPase pump

$$w_{ch} = -5,000 I_{Ca}/F$$
$$w_{pump} = -K_{pump} \frac{[Ca]_i - ca_\infty}{[Ca]_i - ca_\infty + K_{eq}}$$
$$\frac{d[Ca]_i}{dt} = w_{ch} + w_{pump} + (ca_\infty - [Ca]_i)/\tau_r$$

where w_{pump} is the calcium drive through the pump, w_{ch} the calcium drive through the calcium channel Ca_L, ca_∞ = 2.4e-04 mM (equilibrium intracellular calcium concentration), and τ_r = 1e10 ms (time constant of calcium removal by buffering). The time constant τ_r was designed to model a first-order removal of intracellular calcium, which we neglected by setting τ_r to a very large value. K_{pump} = 4e-04 mM/ms (time constant of the ATPase), K_{eq} = 0.02 mM (equilibrium value for the ATPase), and F = 96485.309C mol^{-1} (Faraday constant). If w_{ch} was smaller than 0 then w_{ch} was set to 0 (no inward pumping) [for reference see Destexhe et al. (1993)].

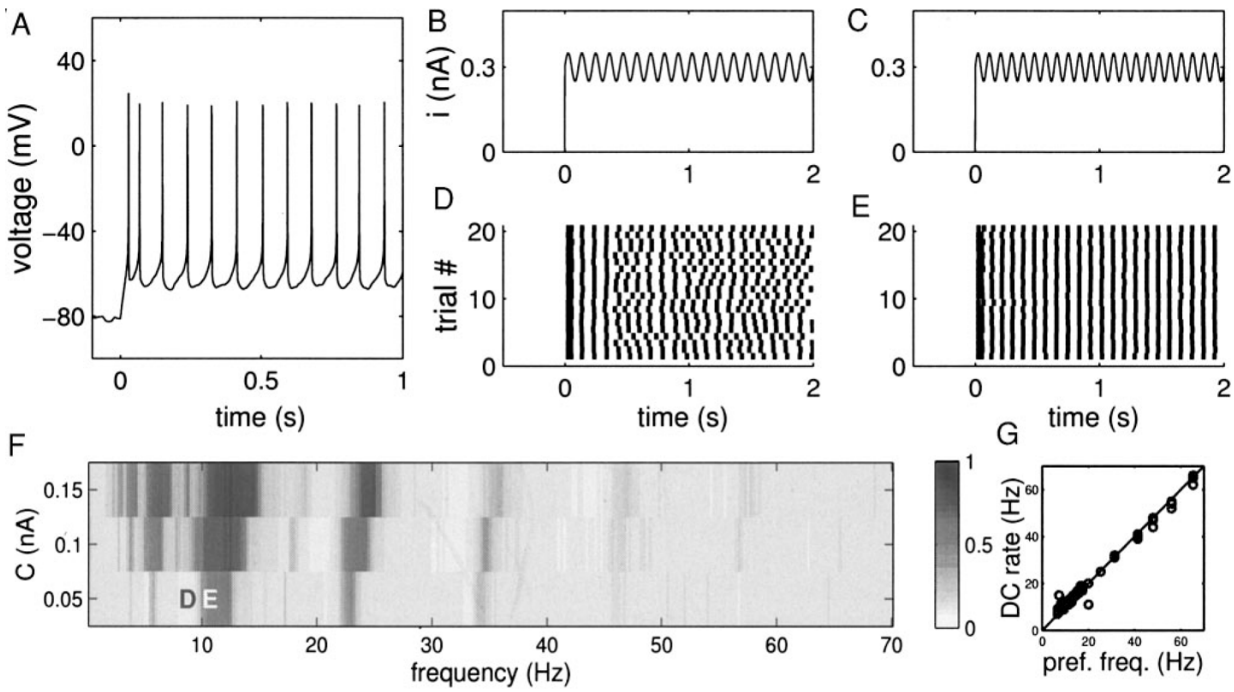

FIG. 1.

Reliability analysis. *A*: voltage response of the reference cell to a current step (I_{DC} = 0.3 nA). *B* and *C*: examples of stimuli (*f* = 9 Hz, *C* = 0.05 nA; *f* = 11 Hz, *C* = 0.05 nA, respectively). *D* and *E*: rastergrams of the spiking responses to the stimuli presented above. Reliability in *D* is low (R_{corr} = 0.10); reliability in *E* is higher (R_{corr} = 0.64). *F*: reliability as a function of frequency *f* and amplitude *C*, of the sine component in the input (Arnold plot, in contrast to all following data calculated with 0.25-Hz resolution, based on 50 trials each). Tongue-shaped regions of increased reliability are visible. Strongest tongue marks the resonant (or preferred) frequency of a cell. Rastergrams underlying reliability at positions D and E are those shown in panels *D* and *E*. *G*: DC firing rate (I_{DC} = 0.3 nA) vs. the preferred frequency for all model cells derived from the reference cell. DC firing rate is a good predictor of the preferred frequency.

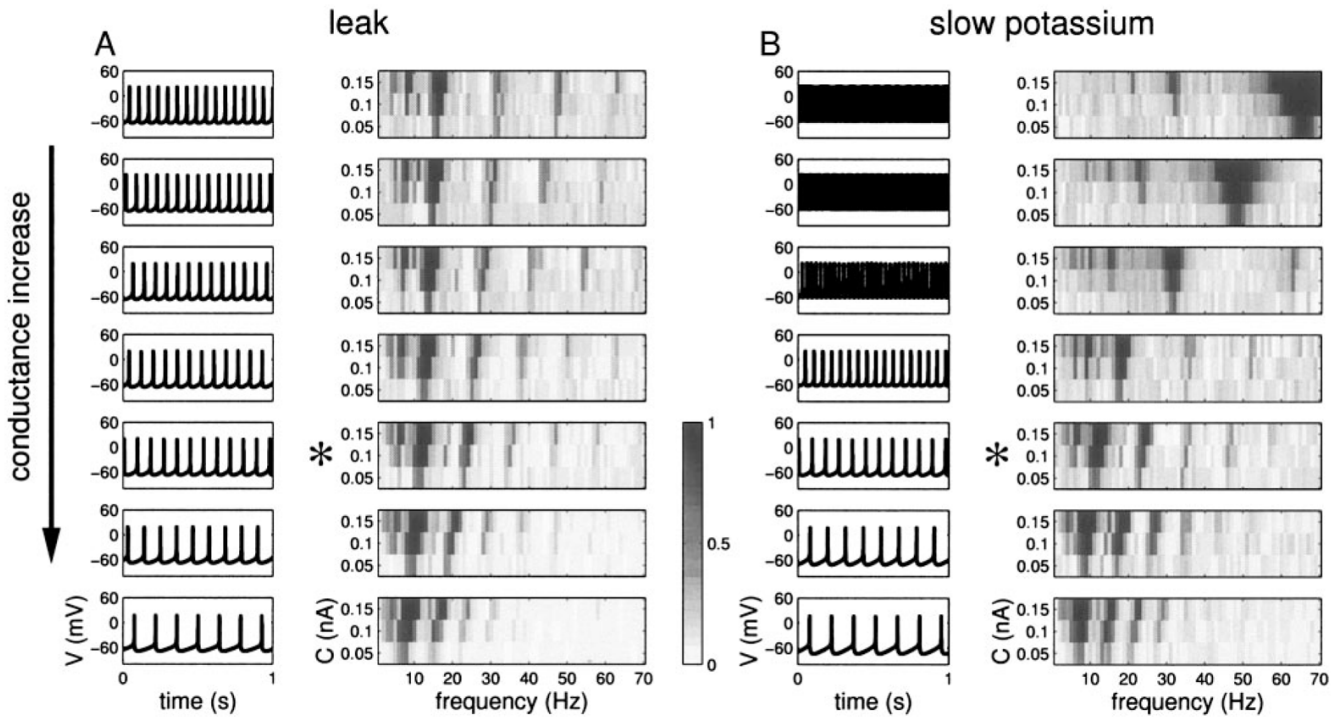

FIG. 2.

Influence of leak and slow potassium conductances on spike timing reliability. *A: right column* of *left panel* shows Arnold reliability plots for 7 different model cells, systematically varying in the amount of leak channels present (0, 0.005, 0.01, 0.015, 0.02, 0.03, and 0.04 mS/cm^2, *top to bottom*). *Left column*: spikes of the corresponding cells in response to pure DC stimulation without intrinsic noise. Input resistance changed significantly with leak conductance over several hundreds of MΩ. *B*: Arnold plots and spikes in response to DC stimulation for 7 different model cells with increasing amounts of K_s (0.05, 0.15, 0.3, 0.6, 1.0, 1.5, and 2.0 mS/cm^2, *top to bottom*). Input resistance changed from about 230 to 150 MΩ. For both panels the *3rd plot from the bottom* (*) represented the reference cell (as in Fig. 1*F*).

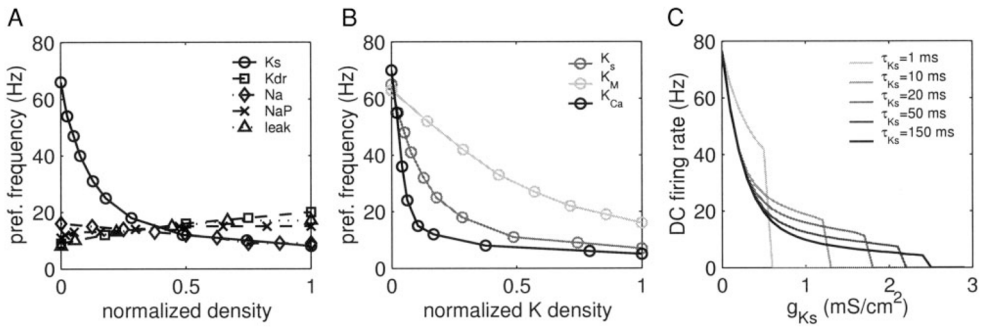

FIG. 3.

Dependency of preferred frequency of the reference cell on individual channel densities. *A*: preferred frequency as a function of normalized channel density (see text for definition), for 5 different conductances. Variation in K_s achieves the broadest shift in preferred frequency. *B*: preferred frequency for variation in a muscarinic potassium channel (K_M) and a calcium-dependent potassium channel (K_{Ca}) as a function of normalized channel density (based on sine wave reliability analysis). K_M and K_{Ca}, respectively, replaced K_s in the reference cell. *C*: DC firing rate (an estimate of the preferred frequency) for K_s channels of different time constants (τ_{Ks}) as a function of K_s peak conductance. Densities are not normalized in this panel. Lowest achievable frequency (at I_{DC} = 0.3 nA) depended on τ_{Ks}.

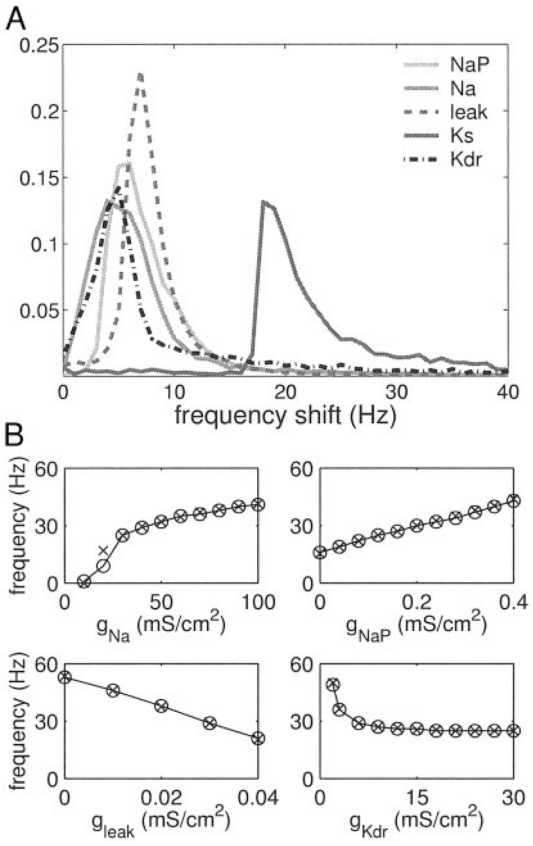

FIG. 4.

Influence of parameter variation on the preferred frequency. *A*: normalized distribution of frequency shifts (maximum changes in firing rate) achievable by one ion channel type (measured over all combinations of the other 4 channel types). Cells in conductance space that did not fire were discarded. Different curves correspond to different ion channel types. *B*: 4 examples of cells where Na, Na_P, K_{leak}, and K_{dr} could mediate large changes in preferred frequency (for parameters see APPENDIX). Circles and solid lines indicate the preferred frequency derived with the sine wave protocol (C = 0.05 nA); crosses indicate DC firing rate.

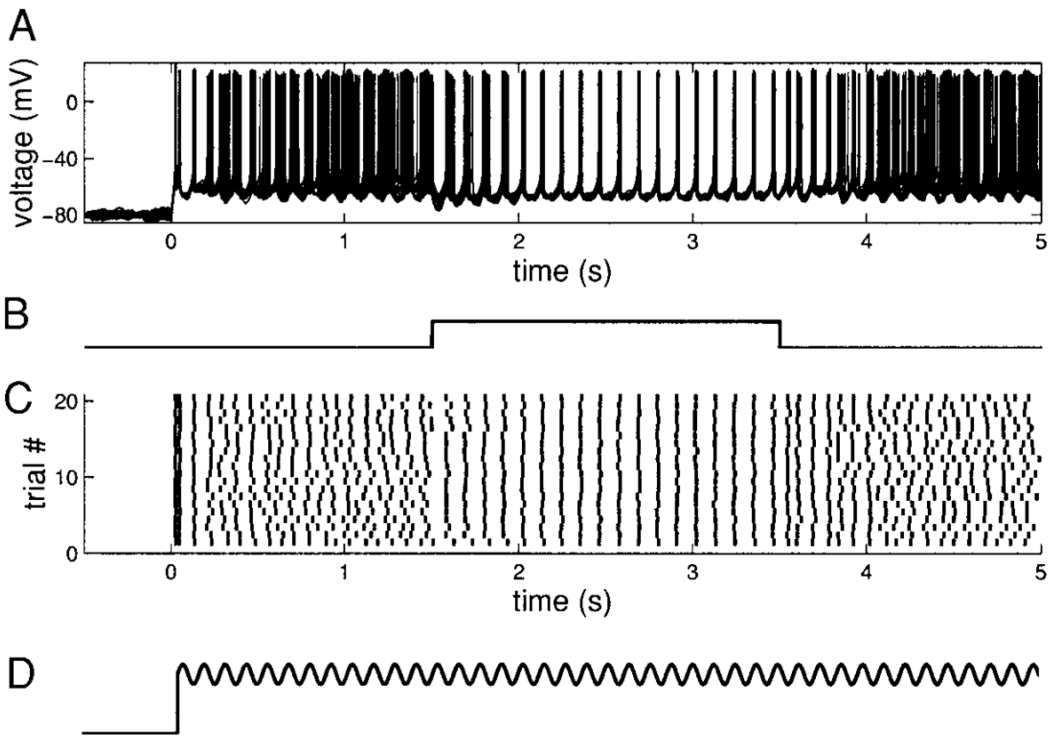

FIG. 5.

Dynamic changes in spike timing reliability attributed to conductance steps. *A*: superimposed voltage traces ($n = 20$) in response to a sine wave ($f = 9$ Hz, $C = 0.05$ nA), which is shown in *D*. K_s conductance was temporarily increased, as indicated in *B*. *C*: rastergram of the responses. Parameters of the cell were those of the reference cell; g_{Ks} values were 0.9 and 1.4 mS/cm^2; noise SD $\sigma = 0.03$ nA. Reliability (here estimated with $\sigma_t = 3$ ms) changed from 0.18 to 0.57 at the conductance step and back to 0.17.

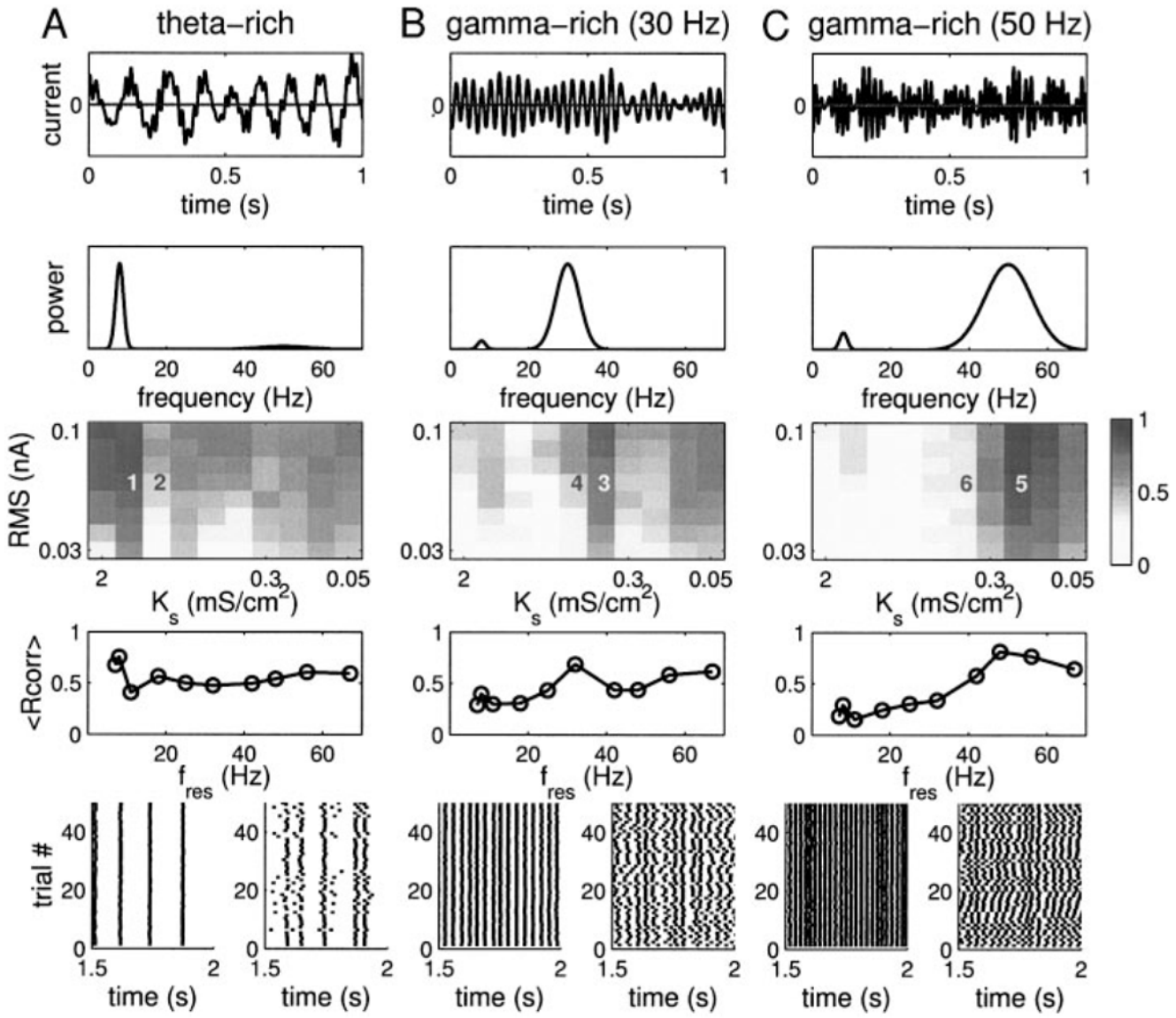

FIG. 6.

Spike timing reliability tested for 3 different inputs: a theta-dominated waveform (*A*) and 2 gamma-dominated waveforms (*B* and *C*). *Top most panel* (in each column): 1 s of the respective stimulus waveform. *Second panel from top*: corresponding power spectrum. *Below*: gray-scale coded reliability is presented as a function of the K_s conductance (horizontal axis) for 8 different RMS values of an input (0.03– 0.1 nA, vertical axis). Panels above the rastergrams show reliability averaged over all RMS values as a function of the preferred frequency (corresponding to the K_s values). *Bottom rastergrams*: 500 ms of the responses behind the numbered positions in the gray-scale coded reliability panels (1 to 6, *left to right*).

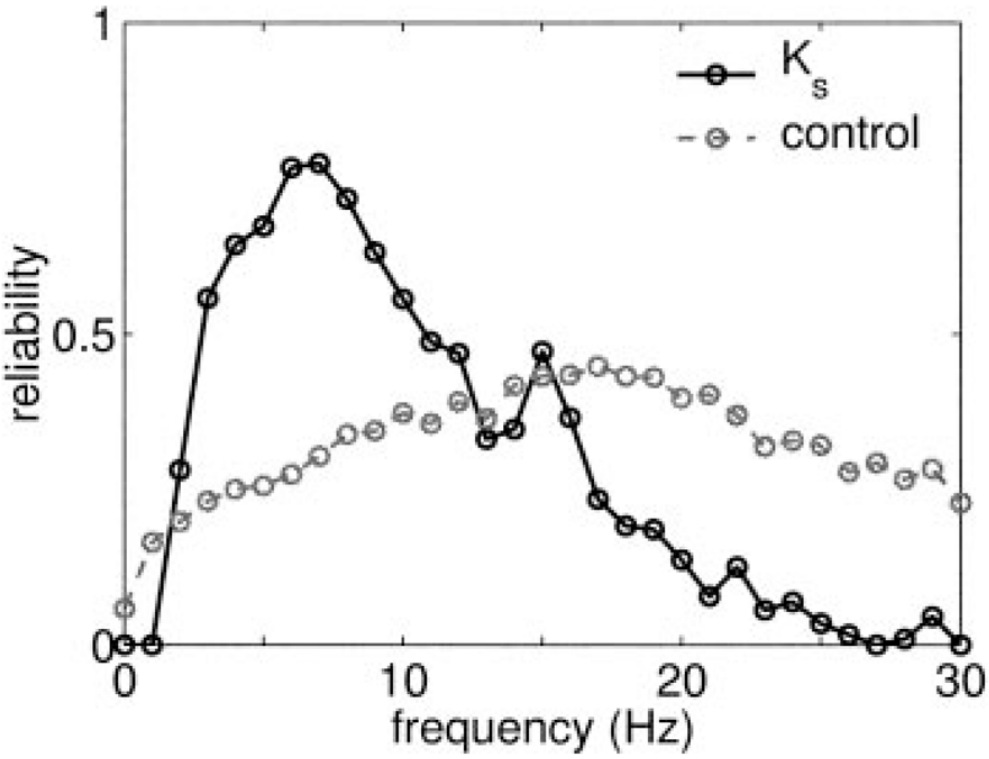

FIG. 7.

Reliability as a function of frequency for a cortical neuron. Gray curve shows reliability in the control case (no additional K_s present). Black curve shows reliability with dynamic clamp recordings, where additional amounts of K_s were present.

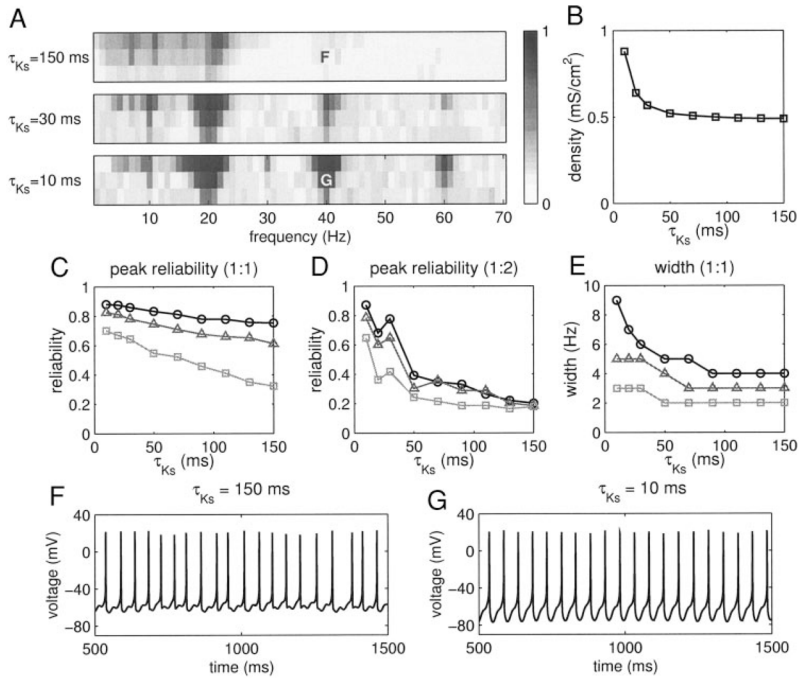

FIG. 8.

Differential reliability at identical preferred frequencies. *A*: Arnold plots for examples of 3 cells differing in the values of τ_{Ks} (as indicated) and slow potassium peak conductance g_{Ks}. K_s conductance was adjusted such that all of them had a DC firing rate of 20 Hz (*B*), i.e., the same preferred frequency. *C*: peak reliability at the preferred frequency (1:1 mode locking) as a function of the K_s time constant for the 3 different amplitudes of the sine component. *D*: peak reliability at the 1st harmonic (1:2 mode locking). For *C* and *D* the SD of the reliability estimate was smaller than or equal to the symbol size. *E*: width of the reliability peak around the preferred frequency. Measured as the width (in Hz) at 50% height between the peak and background reliability levels (mean of reliability from 27 to 29 Hz). SD of the estimate was never greater than 1 Hz for all points presented. Plateaus are attributed to the 1-Hz discretization of the frequency axis. *F* and *G*: sample *voltage traces* of neurons with a slower and a faster potassium channel, respectively (see labeling in *A*). Input to both cells had a frequency of the 1st harmonic (1:2 mode locking). Noise was identical for both cells.

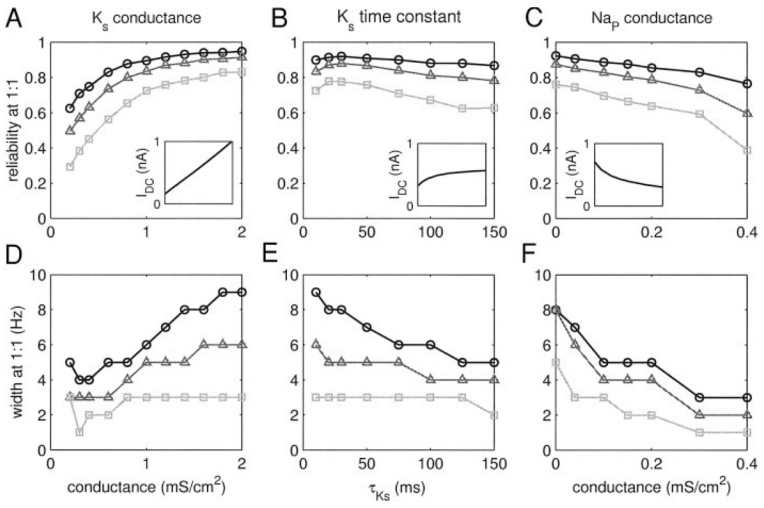

FIG. 9.

Influence of g_{Ks}, τ_{Ks}, and g_{NaP} on reliability at the preferred frequency. Peak reliability at the preferred frequency is presented for neurons differing in g_{Ks} (*A*), τ_{Ks} (*B*), and g_{NaP} (*C*). Different curves correspond to different amplitudes of the sine component. SD of the reliability estimate does not exceed the symbol size. *Insets* indicate how the DC was adjusted to keep the firing rate constant (the *x*-axis of the *insets* is equal to that of the respective panel). See text for a more detailed description of the analysis. *Bottom panels*: depict the widths of the 1:1 reliability peak. SD of this estimate was never greater than 1 Hz. Altogether, more and faster K_s channels enhance reliability, whereas Na_P channels impair reliability.